AGU PUBLICATIONS

JGR

Journal of Geophysical Research: Oceans

RESEARCH ARTICLE

10.1002/2014JC010673

Key Points:
- Relationship found between shear, stratification, and turbulence
- Vertical length scale found to vary inversely with buoyancy frequency
- Resolving the vertical structure of flow features is essential

Correspondence to:
K. J. Richards,
rkelvin@hawaii.edu

Citation:
Richards, K. J., A. Natarov, E. Firing, Y. Kashino, S. M. Soares, M. Ishizu, G. S. Carter, J. H. Lee, and K. I. Chang (2015), Shear-generated turbulence in the equatorial Pacific produced by small vertical scale flow features, *J. Geophys. Res. Oceans*, *120*, 3777–3791, doi:10.1002/2014JC010673.

Received 23 DEC 2014
Accepted 6 MAY 2015
Accepted article online 9 MAY 2015
Published online 27 MAY 2015

Shear-generated turbulence in the equatorial Pacific produced by small vertical scale flow features

K. J. Richards[1,2], A. Natarov[1], E. Firing[2], Y. Kashino[3], S. M. Soares[2], M. Ishizu[1], G. S. Carter[2], J. H. Lee[4], and K. I. Chang[5]

[1]International Pacific Research Center, University of Hawai'i at Mānoa, Honolulu, Hawaii, USA, [2]Department of Oceanography, University of Hawai'i at Mānoa, Honolulu, Hawaii, USA, [3]Research Institute for Global Change, Japan Agency for Marine Earth Science and Technology, Yokohama, Japan, [4]Korean Institute of Ocean Science and Technology, Ansan, Republic of Korea, [5]Seoul National University, Seoul, Republic of Korea

Abstract We investigate the characteristics of shear-generated turbulence in the natural environment by considering data from a number of cruises in the western equatorial Pacific. In this region, the vertical shear of the flow is dominated by flow structures that have a relatively small vertical scale of O(10 m). Combining data from all cruises, we find a strong relationship between the turbulent dissipation rate, ϵ, vertical shear, S, and buoyancy frequency, N. Examination of ϵ at a fixed value of Richardson number, $Ri = N^2/S^2$, shows that $\epsilon \propto u_t^2 N$ for a wide range of values of N, where u_t is an appropriate velocity scale which we assume to be the horizontal velocity scale of the turbulence. The implied vertical length scale, $\ell_v = u_t/N$, is consistent with theoretical and numerical studies of stratified turbulence. Such behavior is found for $Ri < 0.4$. The vertical diffusion coefficient then scales as $\kappa_v \propto u_t^2/N$ at a fixed value of Richardson number. The amplitude of ϵ is found to increase with decreasing Ri, but only modestly, and certainly less dramatically than suggested by some parameterization schemes. Provided the shear generating the turbulence is resolved, our results point to a way to parameterize the unresolved turbulence.

1. Introduction

Unstable shears are an important source of turbulence and the associated mixing in many otherwise stably stratified environmental flows. Such shear-driven mixing can make an important contribution to the dynamics and transport properties of flows and therefore needs to be taken into account in the interpretation of observations as well as in models. Here we will assume the shear generating the turbulence and associated stratification are resolved in measurements or model dynamics, recognizing that this is not always so. In such cases, it is natural to try to relate the turbulent activity to the local gradient Richardson number, $Ri = N^2/S^2$, where N and S are the buoyancy frequency and vertical shear, respectively. Two such examples in the equatorial ocean are *Peters et al.* [1988] (who consider the vertical eddy diffusion coefficient, κ_v) and *Moum et al.* [1989] (who consider the turbulent kinetic energy dissipation rate, ϵ). Both studies find a rapid rise in the respective quantity as Ri decreases below some critical value. This behavior is used to construct parameterization schemes for shear-generated turbulence; a common scheme used in a large number of ocean models is the K-profile parameterization scheme (KPP) of *Large et al.* [1994] which uses a Richardson number based scheme for shear-generated turbulence beneath the surface mixing layer.

As pointed out by *Zaron and Moum* [2009] and others, based purely on dimensional grounds, the turbulence properties need to scale with more than just the Richardson number. In KPP, this is accomplished by scaling the diffusion coefficient resulting from vertical shear by a constant diffusion coefficient. A constant value is obviously undesirable as the conditions under which the turbulence is generated will vary. There have been numerous studies aimed at developing parameterization schemes for shear-driven stably stratified turbulence. Here we mention just two that are based on the concept of a critical Richardson number, Ri_{cr} (see e.g., *Zaron and Moum* [2009] for a more comprehensive review). We require an appropriate length scale L and time scale τ to scale the turbulence properties. *Kunze et al.* [1990] derive an expression for ϵ which can be written in terms of a function of Ri and is nonzero for $Ri < Ri_{cr}$ (see below for details). Written in this way, the parameterization of *Kunze et al.* [1990] employs an $L = \Delta z$, where Δz is the thickness of a layer over which $Ri < Ri_{cr}$, and $\tau = N$, the buoyancy frequency. *Baumert and Peters* [2004] base their scheme

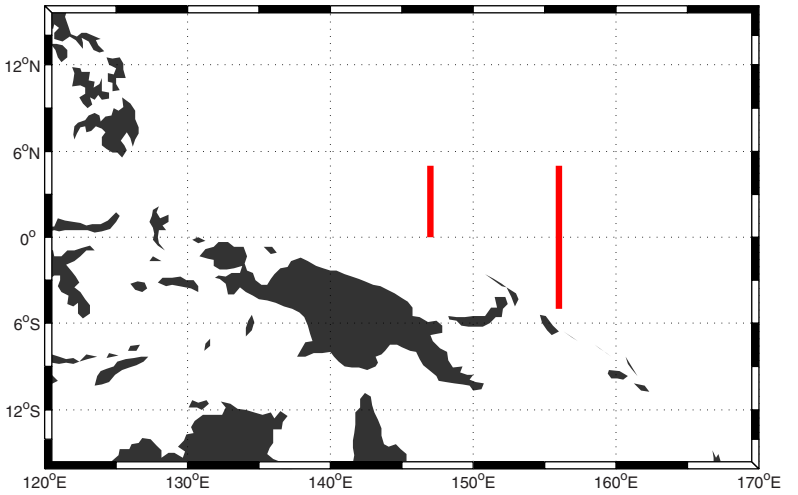

Figure 1. Sections covered by the data: 147°E and 156°E.

on the turbulent kinetic energy, k, and ϵ. They define *master* length and time scales as $L \propto k^{3/2}/\epsilon$ and $\tau \propto k/\epsilon$. We mention the *Baumert and Peters* [2004] scheme here because of the inclusion of the loss of turbulent energy caused by the radiation to internal gravity waves and the extension of nonzero turbulence activity above $Ri = Ri_{cr}$. They assume the onset of the collapse of turbulence into *nonturbulence* occurs when $\tau = 2\pi/N$. For $Ri < Ri_{cr} = 0.25$, turbulence is actively generated, while for $0.25 < Ri < 0.5$, the turbulence is in a decaying transient state and completely collapsed for higher Ri.

The model of *Baumert and Peters* [2004] includes the concept of a time scale for the evolution of turbulence and the length scale L. They consider homogeneous turbulence, but the same is true for isolated turbulent events. The numerical experiments of *Smyth and Moum* [2000] of turbulence resulting from Kelvin-Helmholtz instability show the time evolution of various turbulence length scales and that the relative magnitudes of individual length scales change considerably with time. Here we will average observations taken in various stages of the evolution of turbulent events, as do many other studies, to determine *average* properties, but the fact that there will be time variation in these properties needs to be kept in mind.

In this study, we use data collected in the western equatorial Pacific Ocean on a number of cruises. We focus on the characteristics of the turbulence below the surface mixed layer and down to the base of the thermocline. In this region, the generation of turbulence is dominated by the shear associated with small vertical scale, or fine scale, flow features with a relatively restricted vertical scale [*Richards et al.*, 2012]. With appropriate instrumentation, we are able to capture the shear generating the turbulence and to estimate the associated turbulence activity. Matching the resolution of the measurements to the characteristics of the flow is a key element of the study. By considering the relationship between the turbulent kinetic energy dissipation rate, ϵ, and the vertical shear and stratification, we are able to infer the appropriate scaling for the vertical length of the turbulence. As we will see, this scaling is consistent with Direct Numerical Simulation studies of stratified turbulent flows.

2. Data

Data were collected from a number of cruises to the western equatorial Pacific along two meridians, 156°E (5°S–5°N) and 147°E (equator to 5°N) (see Figure 1). We utilize data from four cruises: R/V Mirai cruises MR09-04 (November/December, 2009), MR10-07 (December 2010), and MR12-03 (July/August 2012), and R/V Kilo Moana cruise KM1225 (November 2012). The cruises occurred in various states of the El Niño, Southern Oscillation (ENSO): positive, negative, neutral, and neutral, respectively, based on the Multivariate ENSO Index (MEI).

Similar instrumentation was used on all cruises. High vertical resolution velocity data were collected using a 600 kHz Teledyne RDI Workhorse Acoustic Doppler Current Profiler attached to a CTD frame and operated

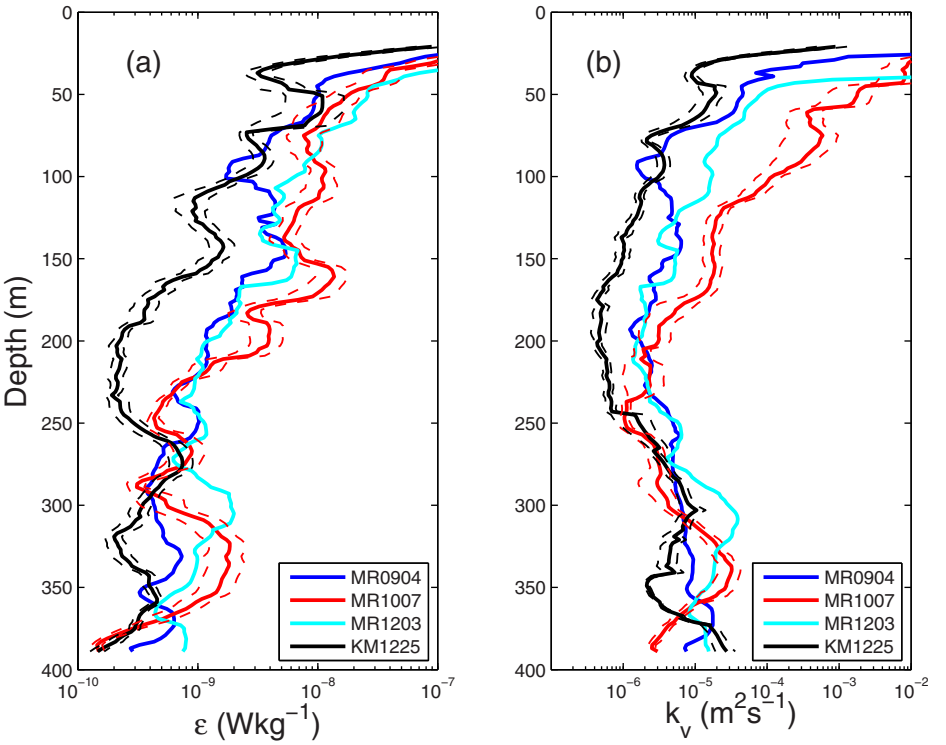

Figure 2. Cruise average vertical profiles of (a) turbulent kinetic energy dissipation rate, ϵ, and (b) vertical diffusion coefficient, κ_v. A 10 m running mean has been applied to individual profiles before averaging. Dashed lines indicate the standard error of the mean based on the variation of individual profiles for cruises MR1007 and KM1225.

in lowered mode (LADCP). Turbulence measurements were taken using a TurboMap-L Microstructure Profiler (MSP), equipped with two fast response shear probes, a slow and fast response temperature probe and a conductivity cell. The station spacing on all sections was a nominal 0.5° of latitude, with station depths ranging from 500 m to 800 m. Each station consisted of a single CTD/LADCP cast followed by one or more MSP casts. Here we use only the first MSP cast to minimize the time difference with the CTD cast (typically 20–30 min). In addition, a time series of CTD/LADCP/MSP casts every 3 h was taken on the equator at 156°E on MR10-07 and MR12-03 (24 h duration) and KM1225 (14 days duration).

The ping rate for the LADCP was set at 4 per second and the depth cell size to 2 m depth. With this cell size, the range of the instrument varied from 20 m to 40 m depending on the availability of scatterers. Single-ping profiles were assembled into a velocity profile using a new implementation of the shear method [*Fischer and Visbeck*, 1993] as described by *Polzin et al.* [2002]. To reduce the effect of the package's wake, which becomes increasingly important for higher-frequency sonars, the wake interference is detected based on its signature bias in the top several depth cells. In each such affected single-ping profile, a 3-beam solution, omitting the down-stream beam, replaces the usual 4-beam solution for the horizontal and vertical velocity components.

The turbulent kinetic energy dissipation rate, ϵ, is calculated from the microstructure shear measurements by integrating the wavenumber spectrum [*Shay and Gregg*, 1986; *Peters et al.*, 1988] from 50% overlapping 2 db bins. Following *Wesson and Gregg* [1994], the empirical Nasmyth spectrum [*Oakey*, 1982] is used to account for missing variance. Here rather than using a fixed cutoff wavelength like *Wesson and Gregg* [1994], we use an iterative approach to identify where the spectrum is dominated by noise. The wavenumber interval used in the integration is increased in small increments (2 cpm) and the resulting value is compared to the expected value over this range from the Nasmyth spectra fitted to the previous integration limits. If the values diverge by more than a factor of 5 in ϵ, a second larger interval is tested to determine if it is the noise spectrum or simply a transient departure.

Salinity for the MSP was calculated using the conductivity measurement and the temperature from the slow probe. To minimize salinity spiking, we applied a lag to the temperature measurement. The lag was

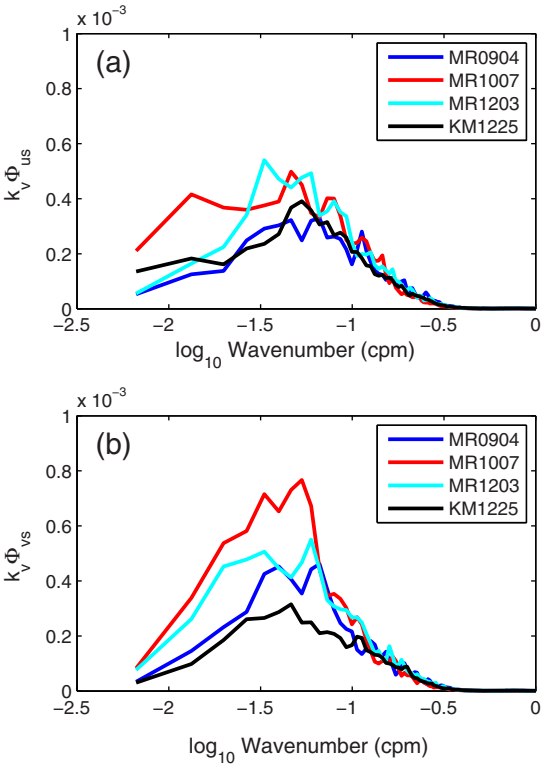

Figure 3. Cruise average vertical shear spectra Φ_u and Φ_v for the (a) zonal and (b) meridional components of velocity, respectively, in the depth interval 100–250 m for individual cruises. Spectra are plotted in variance preserving form, where k_v is the vertical wavenumber (in cpm).

calculated by minimizing the variance in salinity after a high-pass filter, O(10 m), was applied to the vertical profile of each cast. The estimated lag was O(0.5 s) and was consistent between casts on individual cruises. The MSP salinity was made consistent with that from the CTD by ensuring the depth average between 200 and 300 m was the same when averaged over all casts of a given cruise.

All data are binned on 2 m depth intervals to match the resolution of the LADCP measurement of velocity. The prime variables used in the analysis below are ϵ, S^2, and N^2. Vertical profiles of these variables from an individual cast of the CTD/LADCP and the subsequent MSP cast are aligned on density and mapped back to the depth of density from the MSP cast. The effectiveness of this alignment is demonstrated by the fact that both the magnitude and depth of N^2 extrema from the CTD and MSP are very similar.

We consider turbulence below the surface mixed layer. We define the depth of the mixed layer to be the depth at which the change in density from that at the surface is 0.02 kg m^{-3}. Comparison with ϵ shows that this definition more than adequately captures the depth to which surface-induced turbulence penetrates.

3. Results

The cruise average vertical profile (i.e., the average of all profiles taken on a particular cruise) of the turbulent kinetic energy dissipation rate, ϵ, is shown in Figure 2a. The vertical diffusion coefficient, κ_v, is estimated by $\kappa_v = \gamma\epsilon/N^2$, where γ is the mixing efficiency and N the buoyancy frequency [*Osborn*, 1982]. While recognizing that the mixing efficiency may vary with time in an evolving flow [*Smyth et al.*, 2001; *Peltier and Caulfield*, 2003], here we will take γ to be constant with the usual value of 0.2. Cruise average profiles of κ_v are shown in Figure 2b.

There are distinct differences between cruises with regard to the level of turbulence activity and the associated vertical diffusion coefficient, but in all cases there is a general decrease with depth in both ϵ and κ_v down to ~200 m. This depth corresponds approximately to the bottom of the thermocline (defined loosely as the maximum depth at which N^2 falls below $\sim 2 \times 10^{-4}$ s^{-2}) which is in general around 200–250 m depth [see e.g., *Richards et al.*, 2012, Figure 3]. At greater depths, three out of four of the cruise averages show distinct maxima in both ϵ and κ_v [see also *Richards et al.*, 2012, Figure 2b]. These elevated values at depth are restricted to profiles taken within less than 2 degrees of the equator and may be associated with the near-equator elevated values estimated from Argo data by *Whalen et al.* [2012].

As pointed out by *Richards et al.* [2012], the turbulence activity within and above the thermocline tends to be associated with flow structures with relatively small vertical scale (we will refer to these flow features as SVSs), rather than the larger scale currents in the region. The cruise average vertical shear spectra Φ_u and

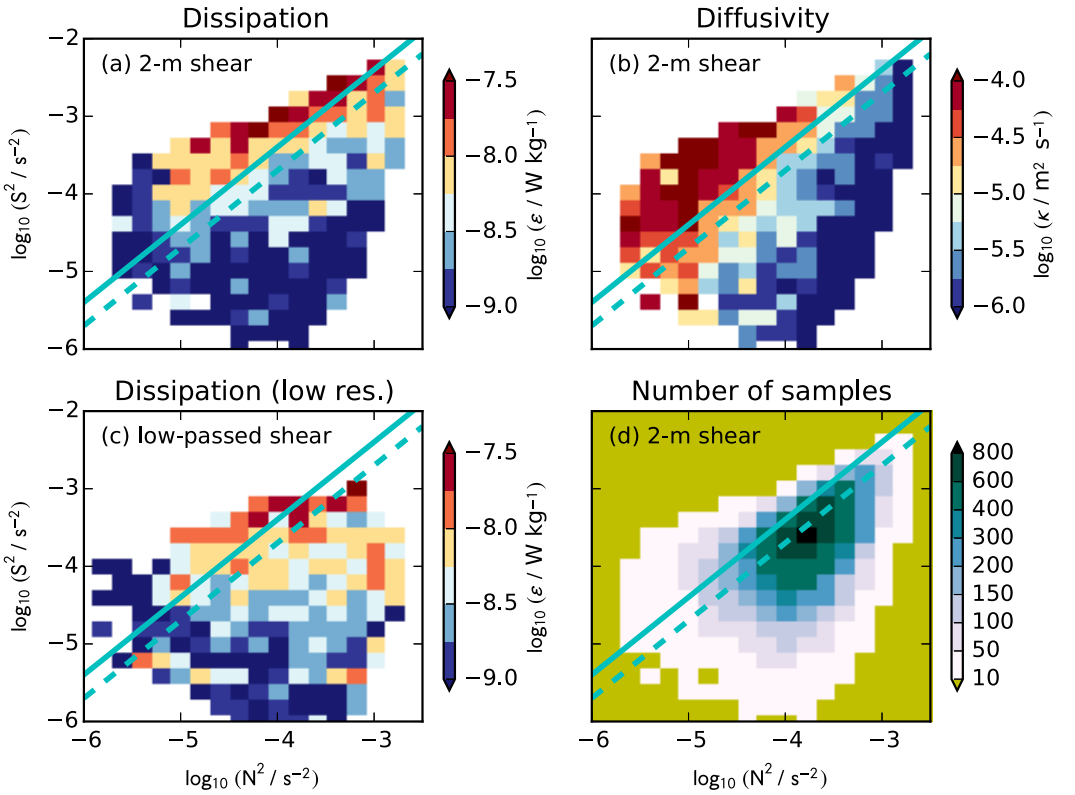

Figure 4. (a) Turbulent kinetic energy dissipation rate, ϵ, bin averaged with respect to $\log_{10}(S^2)$ and $\log_{10}(N^2)$. (b) As for Figure 4a but for the vertical diffusion coefficient κ_v. (c) As for Figure 4a but ϵ bin averaged with respect to $\log_{10}(S_f^2)$, where S_f is the vertical shear of currents after a low-pass Fourier filter has been applied. (d) Number of points in each bin average. Shaded area indicates bins that have 10 or more samples. In each plot, solid cyan line $Ri = 0.25$; dashed cyan line $Ri = 0.5$. Plotted data restricted to bins that have 10 or more samples.

Φ_v for the zonal (u) and meridional (v) components of velocity, respectively, in the depth interval 100–250 m are shown in variance preserving form in Figure 3. The spectra are peaked (particularly Φ_v) at a vertical wavelength of 20–30 m, with the spectra falling off sharply with wavenumber for smaller vertical scales. For MR1007, the peak in Φ_v has a distinctly larger value than for Φ_u. This dominance in v is restricted to less than 2 degrees from the equator (except one profile at 3.5°N, 147°E) and is consistent with the expected small-scale structures associated with inertial instability [*Richards and Edwards*, 2003].

3.1. Relationship Between ϵ, S^2, and N^2

To examine the relationship between the resolved shear, stratification, and turbulence, the turbulent kinetic energy dissipation rate, ϵ, and the vertical diffusion coefficient, κ_v, from all profiles and all cruises are binned with respect to the associated values of $\log_{10}(S^2)$ and $\log_{10}(N^2)$, where $S^2=(du/dz)^2+(dv/dz)^2$ (Figures 4a and 4b, respectively). Here we have taken N calculated from data from the Turbomap microstructure probe, although very similar distributions are found if we use N calculated from the CTD data (again demonstrating the effectiveness of the profile alignment). Data are restricted to the depth interval from the base of the mixed layer to 250 m (approximately the depth of the base of the thermocline). For KM1225, we further restrict the maximum depth to 100 m. The majority of measurements on KM1225 were taken at the equator and ϵ was found to be significantly lower than on other cruises (Figure 2). Here below 100 m, the buoyancy Reynolds number, $\mathcal{R}=\epsilon/(\nu N^2)$ (where ν is the kinematic viscosity), was well below 20 and the flow is deemed to be in a nonturbulent double-diffusive regime using the criterion of *McDougall and Ruddick* [1992] and *Lee et al.* [2014].

The number of samples in each bin is shown in Figure 4d. The ridge of the distribution is aligned more or less along a Richardson number equal 0.5.

The pattern of high ϵ in (S^2,N^2) space is very striking. High values of ϵ occur for low Richardson number, $Ri = N^2/S^2$ ($Ri = 0.25$ and 0.5 are shown). Moreover, for a given value of Ri, there is reduction in ϵ as N^2 (and

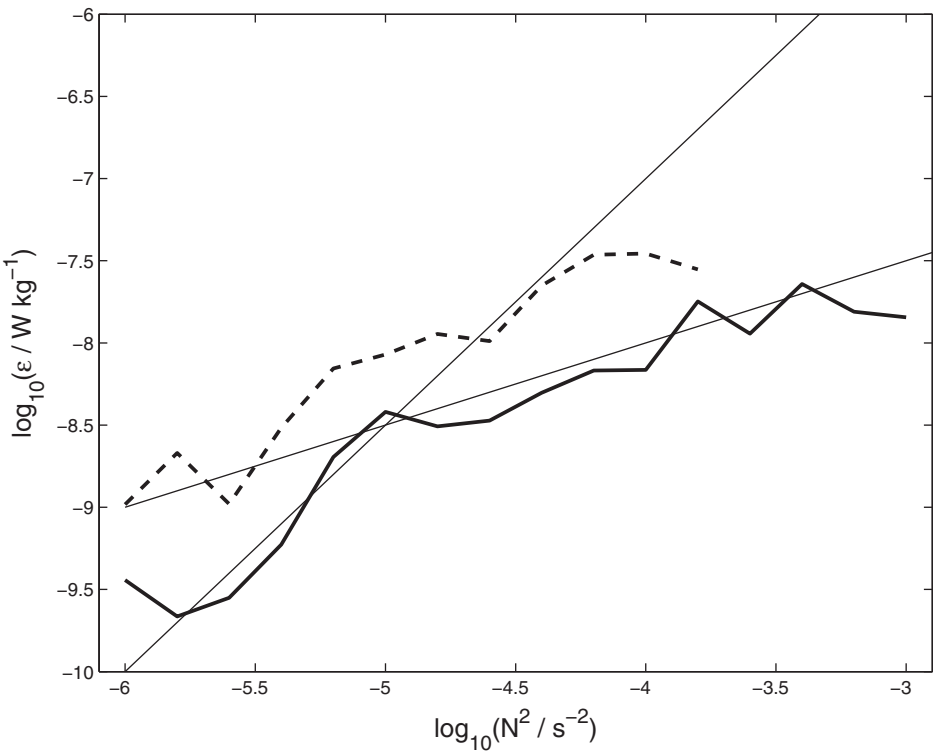

Figure 5. Turbulent kinetic energy dissipation rate, ϵ, plotted against $\log_{10} N^2$ for Richardson number, *Ri*, in the interval 0.2–0.3 (solid line) and 0–0.1 (dashed line). Data taken between the mixed layer and 250 m depth. Thin black lines show ϵ varying as N^3 and N.

equivalently S^2) decreases (*Polzin* [1996] notes a similar reduction). High values of κ_v (Figure 4b) are similarly restricted to low Richardson number, at least for $N^2 > 10^{-5}$ s^{-2}, but now κ_v decreases for *increasing* N^2 for a fixed *Ri*.

The distribution of ϵ in (S^2,N^2) space is very dependent on the vertical resolution of the observations. To illustrate, Figure 4c shows ϵ binned with respect to (S_f^2, N^2), where S_f is the shear calculated after a low-pass Fourier filter has been applied to the vertical distribution of the horizontal components of velocity. We have taken the cutoff to have a vertical wavelength of 30 m (inverse wavenumber ∼5 m) which corresponds approximately to the peak in the shear spectra shown in Figure 3. The impact is dramatic. High ϵ is no longer so tightly restricted to low Richardson number. The peak in the distribution of the number of samples in each bin is shifted to $Ri = 2.5$ (not shown). The lesson is clear. Resolving the shear associated with the SVSs is vital to establish the relationship between flow features and the turbulence generated by them. (We note the sensitivity to vertical resolution we find in the western equatorial Pacific is much greater than that found by *Smyth and Moum* [2013] in the eastern equatorial Pacific—cf. their Figure 2).

The value of ϵ below 250 m depth has a similar character to that above in that higher values are restricted to small *Ri* and high S^2 (as in Figure 4a) but the amplitude is lower by a factor of 2–5 (not shown). Here the stratification and SVS activity are in general weaker. We return to this point later.

To examine the variation of ϵ at a fixed value of *Ri*, further we calculate the average ϵ in a band of *Ri* of width 0.1 centered on $Ri = 0.25$ for varying N^2 by taking an arithmetic mean of samples in a given (Ri, $\log_{10} N^2$) bin (Figure 5). Again, data are taken between the base of the mixed layer and 250 m depth. For $N^2 > 10^{-5}$ s^{-2}, we find ϵ is approximately proportional to N over two decades variation in N^2 (a linear regression gives $\epsilon \propto N^{1.07}$). For $N^2 < 10^{-5}$ s^{-2}, the value of ϵ drops off until the sensitivity of the instrument is reached at approximately $\epsilon = 3 \times 10^{-10}$ W kg^{-1}.

A similar slope ($\epsilon \propto N$) is found for other values of *Ri*, with the amplitude of ϵ increasing as *Ri* decreases. Band-averaged values centered on $Ri = 0.05$ are shown as the dashed line in Figure 5. Again, there is a hint of a roll-off for small N^2. As a measure of the variation of ϵ with *Ri*, we fit the line $log_{10}\epsilon = \log_{10} a + 0.5 \log_{10} N^2$ (i.e., $\epsilon = aN$) for $N^2 > 10^{-5}$ s^{-2} for bands of *Ri* centered on varying *Ri* and plot *a* against *Ri* (Figure 6). We

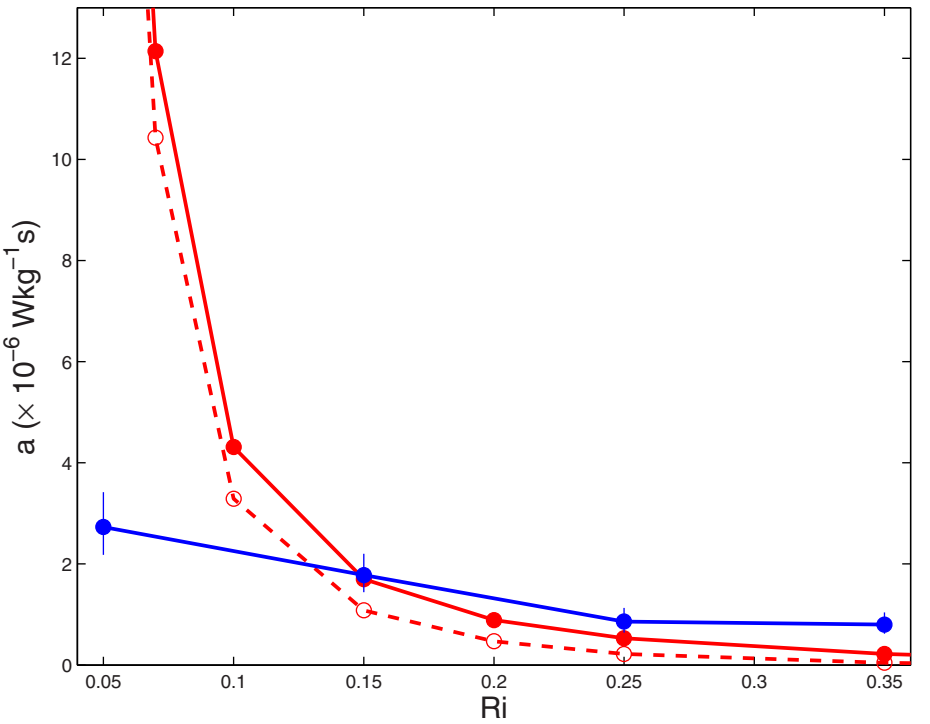

Figure 6. Amplitude, a, of ϵ as a function of Richardson number, Ri, where it is assumed $\epsilon = aN$. Close blue circles: observations. Vertical lines show one standard deviation of the difference between the binned averaged values of ϵ and the fit $\epsilon = aN$. Closed red circles: ϵ_{KWB} with $c\ddot{u} = 0.004$ and $Ri_{cr} = 1$, open red circles: ϵ_{KWB} with $c\ddot{u} = 0.004$ and $Ri_{cr} = 0.5$. In all cases, values are averaged over a band of Ri which is 0.1 wide.

plot only points for which a full linear fit gives a slope within 20% of 0.5. Also shown is one standard deviation of the difference between the binned averaged values of ϵ (in a given Ri band) and the fit $\epsilon = aN$. The amplitude a increases with decreasing Ri, although not in a particularly dramatic way in comparison with existing parameterizations [e.g., *Kunze et al*., 1990] (see section 3.3 for a detailed comparison). Note the variation is somewhat smoothed by the width of the Ri band. The value of a at $Ri = 0.05$ is only a factor of 3 greater than that at $Ri = 0.25$. There is a very slight (2%) reduction in a going from $Ri = 0.25$ to $Ri = 0.35$. There is a much larger reduction (55%) with $Ri = 0.45$, although now the slope of a linear fit ($= -0.06$) is very different from 0.5.

Assessing the uncertainty in the estimates of bin-averaged values of ϵ, such as those shown in Figure 5, is difficult. The principal problem is that the level of noise affecting the estimate of ϵ is not too different from the signal, particularly for smaller values of N^2 (see Figure A1). We discuss the issues and provide our best guess for the confidence limits in Appendix A derived from a one-sided Gaussian fit. Using the mean confidence limit, we estimate that $\epsilon \propto N^{1.07 \pm 0.18}$ where the 95% confidence limits on the slope result from a Monte Carlo simulation. Confidence is further gained from the fact that we consistently find $\epsilon \propto N$ for a range of Ri (0.05–0.35).

3.2. Scaling of the Turbulence

The observed variation of $\epsilon \propto N$ for a fixed value of Ri (Figure 5) has implications for the scaling of the turbulence. If the variables determining ϵ are N, S, and an unknown length scale ℓ_v then a dimensionally correct expression for ϵ can be written as

$$\epsilon = \ell_v^2 N^3 f(Ri) \tag{1}$$

where $f(Ri)$ is a yet to be determined function of the Richardson number, Ri. An equivalent choice would be $\epsilon = \ell_v^2 S^3 g(Ri)$, where the unknown function $g(Ri) = Ri^{1.5} f(Ri)$. A similar dimensional scaling is got by *Kunze et al*. [1990] based on physical reasoning (see expression (6)). Note that in the special case $f(Ri) = 1$, the length scale ℓ_v is the Osmidov scale, $L_O = \sqrt{\epsilon / N^3}$ (the vertical scale at which buoyancy forces inhibit vertical

motions). If $f(Ri)=Ri^{-3/2}$ then ℓ_v is the Corssin scale, $L_C=\sqrt{\epsilon/S^3}$ (the scale at which the large-scale shear deforms turbulent eddies).

Our observation that $\epsilon \propto N$, for a fixed value of Ri, then implies the length scale ℓ_v varies as

$$\ell_v = \frac{u_t}{N} \tag{2}$$

where u_t is a velocity scale. Taking u_t to be the horizontal velocity scale of the turbulent flow then the scaling in (2) is the same as that found in a number of studies on stratified turbulent flows with ℓ_v being the vertical scale of the turbulent flow [e.g., *Godeferd and Staquet*, 2003; *Waite and Bartello*, 2004; *Brethouwer et al.*, 2007].

Brethouwer et al. [2007] point out that the scaling for ℓ_v depends on the parameter $\mathcal{R}_h=ReF_h^2$, where the Reynolds number, $Re=U\ell_h/\nu$, the horizontal Froude number, $F_h=U/(\ell_h N)$, and ν and ℓ_h are the kinematic viscosity of the fluid and horizontal length scale, respectively. Assuming $\ell_h \propto U^3/\epsilon$ [*Taylor*, 1935] then $\mathcal{R}_h$ can be written as

$$\mathcal{R}_h = \frac{\epsilon}{\nu N^2} \tag{3}$$

i.e., $\mathcal{R}_h$ is equivalent to the buoyancy Reynolds number, $\mathcal{R}$. In the strong limit, defined as $\mathcal{R} \gg 1$, ℓ_v scales as (2). In the weak limit, $\mathcal{R} \ll 1$, viscosity dominates and ℓ_v becomes independent of N. *Bartello and Tobias* [2013] suggest the scaling for ℓ_v departs from the strong limit for $\mathcal{R} \lesssim 10$. The majority of the observed turbulence in the present study is in the strong regime although things become marginal when ϵ drops below 10^{-9} W kg^{-1} and $N^2 \gtrsim 10^{-4}$ s^{-2}. For KM1225 below 100 m depth, in general, $\mathcal{R} \ll 10$ and these data have been discarded from the present analysis (as discussed above).

For reference, we have included the line $\epsilon \propto N^3$ in Figure 5, the expected variation at a fixed value of Ri if ℓ_v is constant (1). The data for $N^2 > 10^{-5}$ s^{-2} are far from this line. Although the data show a falloff in ϵ for $N^2 \lesssim 10^{-5}$ s^{-2}, we do not place much confidence in the apparent coincidence with $\epsilon \propto N^3$ as this may be an artifact of averaging close to the noise level of the instrument (see Appendix A).

Assuming the turbulence is driven by the shear of the SVSs then we expect the turbulent velocity u_t to be O(0.1) times the amplitude of the SVSs, $\tilde{u}$. The factor 0.1 is expected to be a rough upper bound with substantially smaller values as the turbulence grows and decays [see e.g., *Smyth et al.*, 2005, Figures 2 and 3; *Koop and Browand*, 1979, Figure 12]. As a quantitative measure of SVS activity, we define $\tilde{u}$ as the root-mean-square of u between 50 and 250 m after a high-pass Fourier filter has been applied (with a cut-off wavelength of 50 m to capture the peak in the shear spectrum; the results are not overly sensitive to the precise cutoff used). Defined in this way, there is only a modest variation in the average value of $\tilde{u}$ between cruises. Averaging over all profiles for a given cruise, we find $\tilde{u}$ varies from 0.047 for MR0904 to 0.060 m s^{-1} for MR1007. The average overall cruises gives $\tilde{u} = 0.05$ m s^{-1}. This gives an estimate for $u_t \simeq 0.005$ m s^{-1} (or less). Taking $u_t = 0.005$ m s^{-1}, ℓ_v increases from 0.15 m to 1.5 m as N^2 decreases from 10^{-3} s^{-2} to 10^{-5} s^{-2}. We also note that this crude estimate of u_t implies $f(Ri)$, as in (1), varies from 0.03 to 0.1 as Ri decreases from 0.25 to 0.05 (decreasing u_t by a factor of 2 will increase $f(Ri)$ by a factor of 4).

To consider the scaling of ℓ_v with u_t (and by association $\tilde{u}$), we look briefly at data below the thermocline. Here the average $\tilde{u}$ is 0.03 m s^{-1}, half the value within and above the thermocline. This reduced $\tilde{u}$, and the expected associated reduction in u_t, would imply a factor 4 reduction in ϵ from (1) and (2), in line with the observed reduction in ϵ. It should be noted, however, that the shear spectrum below the thermocline is much flatter so that $\tilde{u}$ does not represent SVS activity at a definite scale.

Combining (1) and (2), the vertical diffusion coefficient, κ_v ($=\gamma\epsilon/N^2$) becomes

$$\kappa_v = \frac{\gamma u_t^2 f(Ri)}{N} \tag{4}$$

i.e., for a fixed Ri, κ_v increases with SVS activity and decreases with N (the latter is seen in Figure 4b).

Expression (1) implies the ratio of the turbulent length scale to Osmidov scale $\ell_v/L_O = 1/f(Ri)^{1/2}$, i.e., the ratio decreases with decreasing Ri (Figure 6: noting that $a=u_t^2 f$). We note that a similar conclusion was drawn by *Rohr et al.* [1988] from laboratory experiments when considering the ratio L_t/L_O, where L_t is based on the Ellison scale, $-\rho'/(\partial\bar{\rho}/\partial z)$ (and $\bar{\rho}$ and ρ' are the time mean and fluctuating density, respectively),

although they find a somewhat larger decrease as Ri varies between 0.25 and 0.05, the decrease being a factor of approximately 4 (their Figure 15). There are several caveats, most notably the use of different turbulence scales ℓ_v and L_t and the different averaging used in the two studies. *Rohr et al.'s* [1988] result is for large times in the evolution of the turbulence in a channel. Here we average across the turbulence in various stages of its evolution.

The geometry of the flow will place an upper bound on the turbulence scales. In our case, we expect this to be the vertical scale of the SVSs that are driving the turbulence, L_S (which, if we take this to be the inverse vertical wavenumber of the SVSs, is ~5 m). This restriction on the outer scales may be in part responsible for the drop-off in ϵ for high N^2 at a fixed value of Ri (Figure 5), through a restriction on the turbulent scale ℓ_v. We discuss this a little further in the next section. We also note that as N^2 decreases, at some point ℓ_v will become comparable with the averaging depth of 2 m, making the 2 m averaged values of S^2 and N^2 inappropriate when considering the scaling. We have not investigated the sensitivity to averaging depth further since a relatively modest degradation in resolution of the shear has a large effect on the relationship between ϵ, S^2, and N^2 (Figure 4c).

3.3. Comparison With KWB

Kunze et al. [1990] (hereafter referred to as KWB) suggest the following estimate of ϵ based on the characteristics of Kelvin-Helmholtz instability:

$$\epsilon_{KWB} = c^2 \Delta z^2 \frac{(S^2 - N^2/Ri_{cr})}{24} \frac{(S - N/Ri_{cr}^{1/2})}{4} \tag{5}$$

when $Ri < Ri_{cr}$ (otherwise $\epsilon_{KWB} = 0$), where Ri_{cr} is a critical Richardson number for active turbulence and Δz is the thickness of a layer over which $Ri < Ri_{cr}$. The first term in parentheses is an estimate of the kinetic energy available for turbulence to mix momentum and density to a state where $Ri = Ri_{cr}$. The second term approximates the linear growth rate of Kelvin-Helmholtz instability. We have introduced the constant c^2.

Peters et al. [1995] and *Polzin* [1996] both find ϵ_{KWB} agrees reasonably well with observations. We note, however, that in both studies, Δz is taken to be equal to the vertical sampling interval of S^2 and N^2, which is contrary to the original definition of KWB. *Polzin* [1996] considers the sensitivity to the sampling interval. Below we show in applying KWB to our data, there is good reason to assume a nonconstant Δz.

Writing (5) in terms of the Richardson number, Ri, we get

$$\epsilon_{KWB} = c^2 \Delta z^2 N^3 f_k(Ri) \tag{6}$$

where

$$f_k(Ri) = \frac{(Ri_{cr} - Ri)(Ri_{cr}^{1/2} - Ri^{1/2})}{96(RiRi_{cr})^{3/2}}$$

(note $f_k(Ri) \propto 1/Ri^{3/2}$ for $Ri \ll Ri_{cr}$).

As before, the observed variation $\epsilon \propto N$ at a fixed value of Ri for a range of N^2 has implications for the length scale in (6), i.e.,

$$\Delta z = \frac{\tilde{u}}{N} \tag{7}$$

where we have chosen the velocity scale to be the amplitude of the SVSs, $\tilde{u}$, which has a mean value of 0.05 m s^{-1}.

The cruise average Δz from observations (as defined by *Kunze et al.* [1990]) with $Ri_{cr} = 0.25$ is plotted against N^2 in Figure 7, where N^2 is taken as the average buoyancy frequency squared within the layer. Also shown is (7) with $\tilde{u} = 0.05$ m s^{-1}. For $N^2 > 10^{-4}$ s^{-2}, the amplitude of the mean Δz is generally in accord with (7) over a decade variation in N^2 (except perhaps for MR1007 which has a larger scatter), although viewed over a wider range of N^2, the variation of Δz is perhaps closer to $1/N^{1/2}$. The small variation between cruises is consistent with the small (~15%) variation of $\tilde{u}$ between cruises when $\tilde{u}$ is used in the scaling for Δz. For smaller values of N^2, and for three of the cruises, Δz plateaus at a value ~6 m. As before, we speculate that this restriction on Δz may be caused by the finite vertical scale of the SVSs, although we note Δz for MR1007 displays no indication of a restriction.

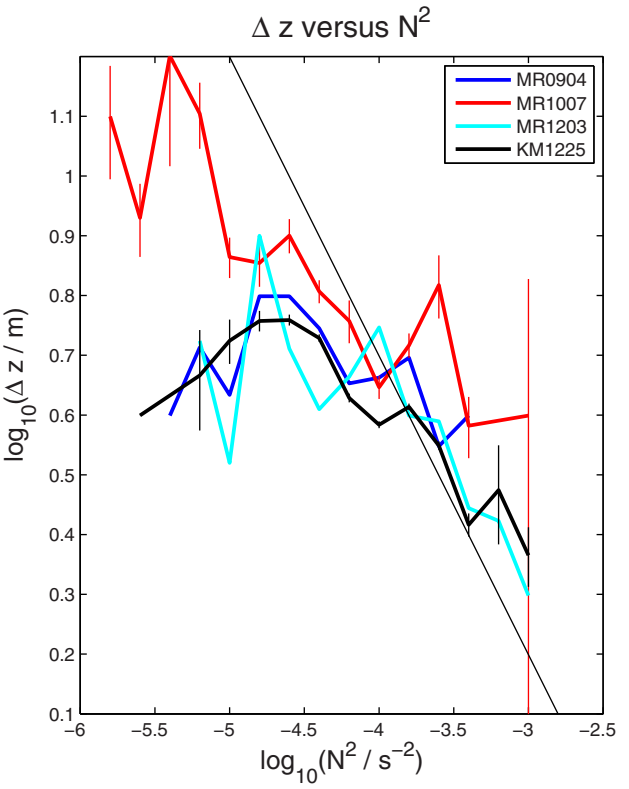

Figure 7. Mean Δz, defined as the thickness of layers with $Ri < Ri_{cr}$ (with $Ri_{cr} = 0.25$), plotted against N^2 for various cruises. Thin black line shows (7) with $\tilde{u} = 0.05$ m s^{-1}.

The variation of ϵ implied by $f_k(Ri)$ in (6) is compared with the observed variation of the amplitude, a, of ϵ with Ri (where it is assumed $\epsilon = aN$) in Figure 6. For consistency, we average (6) over a band of Ri of width 0.1, as we did for the observations. We take Δz given by (7) and $c\tilde{u} = 0.004$. The value of $c\tilde{u} = 0.004$ comes from comparison with the cruise average vertical profiles (not shown). The value of a varies with Ri_{cr}. For $Ri_{cr} = 1$, the value of a implied by (6) is within 35% of the observed value for $Ri = 0.25$ and within 7% for $Ri = 0.15$. For smaller values of Ri, the discrepancy increases markedly. Decreasing Ri_{cr} to 0.5 halves the value of a for $Ri = 0.25$. Obviously, the fit at a given value of Ri can be improved by changing $c\tilde{u}$, but regardless of the parameter settings $f_k(Ri)$ significantly overpredicts the increase in ϵ as $Ri \to 0$. There is also a suggestion that $f_k(Ri)$ falls off too quickly as Ri increases.

The above assumes Δz varies as (7), in which case there is a singularity in ϵ_{KWB} as $N \to 0$. The singularity is avoided if the variation of Δz with N is reduced to $\Delta z \propto 1/N^{3/4}$ (or less).

For sufficiently weak stratification, the vertical scale is expected to be more associated with the Corrsin scale, Lc, i.e., become independent of N, or be affected by the geometry of the flow. We note that the behavior $f_k(Ri) \propto 1/Ri^{3/2}$ for $Ri \ll Ri_{cr}$ implies the vertical scale, in this case Δz, is proportional to L_C. The large discrepancy between $f_k(Ri)$ and the observed $f(Ri)$ for small Ri (Figure 6) suggests that stratification is still important for $Ri = 0.05$, at least for $N^2 > 10^{-5}$ s^{-2}.

With $\tilde{u} \simeq 0.05$ m s^{-1}, the above value for $c\tilde{u}$ implies c is O(0.1). While $\tilde{u}$ appears to be an appropriate velocity scale for Δz (expression (7) and Figure 7), the turbulent length scale $\ell_v = u_t/N$ (where $u_t \sim 0.1\tilde{u}$) appears to be a more appropriate length scale for ϵ_{KWB} than Δz (when based on 2 m averages of S^2 and N^2).

3.4. Comparison With KPP

A number of parameterizations of shear-driven turbulence are based on the gradient Richardson number, Ri. One such parameterization commonly used in ocean models is that by *Large et al.* [1994] as a component of their KPP model, namely

$$\kappa_{KPP} = \kappa_o \left(1 - \left(\frac{Ri}{Ri_{cr}}\right)^2\right)^3 \tag{8}$$

for $Ri < Ri_{cr}$, where κ_o is a specified maximum diffusion coefficient usually taken as a constant. *Large et al.* [1994] set $\kappa_o = 50 \times 10^{-4}$ m^2 s^{-1} and $Ri_{cr} = 0.7$.

Comparison with (4) suggests κ_o should be a function of N and an appropriate velocity scale. To compare the parameterization with the observations, we will ignore this fact and bin average κ_v solely with respect

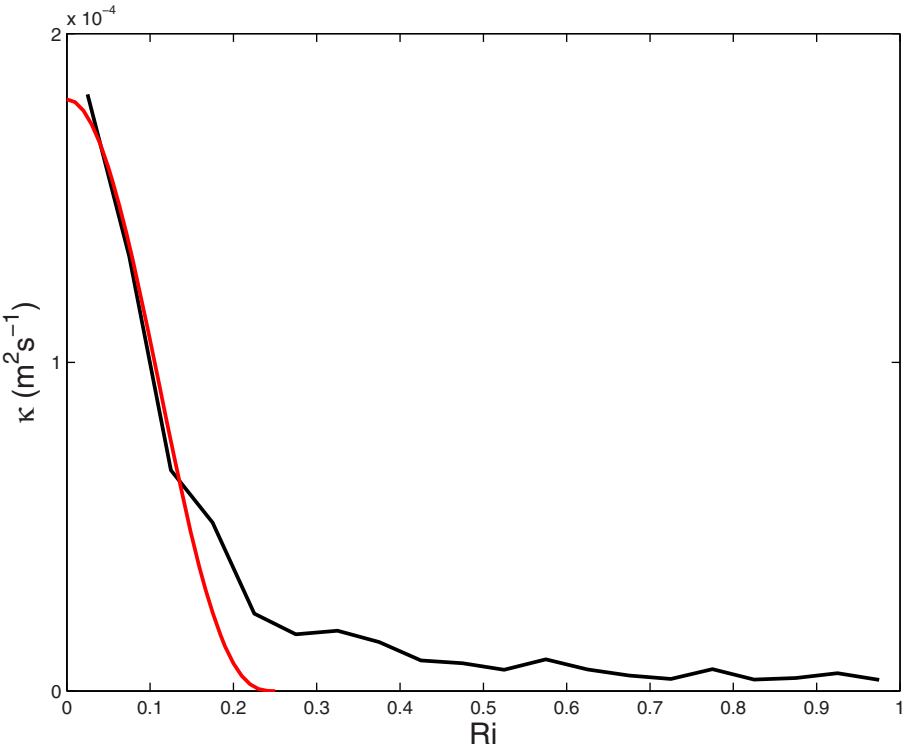

Figure 8. Mean κ_v as a function of Richardson number, *Ri*, alone (black line). Red line: κ_{KPP} with $\kappa_o = 1.8 \times 10^{-4}$ m^2 s^{-1} and $Ri_{cr} = 0.25$.

to *Ri* (as is done in a number of studies) (Figure 8). There is a slow rise in κ_v as *Ri* decreases until $Ri \simeq 0.25$, after which there is sharp rise to a maximum of 1.8×10^{-4} m^2 s^{-1}. This sharp rise in κ for low *Ri* has been seen in a number of observational studies [e.g., *Peters et al*., 1988]. The sharp rise is also mimicked by κ_{KPP} (by construction). Here we have chosen $\kappa_o = 1.8 \times 10^{-4}$ m^2 s^{-1} and $Ri_{cr} = 0.25$, both of which are considerably smaller than the values used by *Large et al*. [1994].

The diffusivity values at low *Ri* contribute most to the mean κ_v. Samples with $Ri \leq 0.25$ contribute 70% to the overall mean κ_v. Samples with $Ri > 0.25$, however, make a significant contribution (30%). It is important, therefore, to account for the tail of the *Ri* distribution ($Ri > 0.25$). We note that increasing Ri_{cr} for κ_{KPP} worsens the fit with observations for higher *Ri*.

4. Conclusions and Discussion

The physical conditions in the thermocline of the western equatorial Pacific are very conducive to studying the properties of shear-generated turbulence. Most of the time, the vertical shear is dominated by relatively small vertical scale flow structures, SVSs, such that the spectrum is highly peaked at around 20–50 m vertical wavelength, and there is a scale separation between the width of the thermocline and the scale of the SVSs. Much of the turbulence in the region is strongly associated with the SVSs rather than the larger scale currents.

With a large number of samples, got by combining measurements from a number of cruises, we are able to examine the distribution of ϵ in (S^2,N^2) space (Figure 4a). High ϵ is confined to low Richardson number. Again, we stress the importance of resolution. We have used 2 m averages in both the velocity (used to calculate *S*) and *N*. When the resolution of the shear is reduced, the tight distribution of ϵ in (S^2,N^2) space is lost (Figure 4c). We are unable to say how things may change with higher resolution, but the sharp dropoff in the shear spectrum for vertical scales less than 20 m (in terms of vertical wavelength: Figure 3) suggests any changes may be modest.

To examine the scaling of ϵ, and κ_v, in more detail, we look to the variation of ϵ at a fixed value of *Ri* (Figure 5). For sufficiently large N^2 (in our case $N^2 > 10^{-5}$ s^{-2}) $\epsilon \propto u_t^2 N$, which implies the vertical scale $\ell_v = u_t/N$. We take the velocity scale u_t to be the horizontal velocity scale of the turbulent flow, which is assumed to be O(0.1 $\tilde{u}$), where $\tilde{u}$ is the (measurable) amplitude of the observed small vertical scale flow features (SVSs). Such behavior is found for $Ri < 0.4$. The vertical diffusion coefficient then scales as $\kappa_v \propto u_t^2/N$ at a fixed value of Richardson number. The scaling for ϵ deduced from our data is consistent with theoretical and numerical studies of stratified turbulence.

In concentrating on the variation of ϵ with N and combining data from a number of cruises, we have assumed that variations in the velocity scale u_t, at least on average, do not change significantly between the various cruise data sets. Indeed, this is the case in the thermocline if we assume u_t is associated with the amplitude of the SVS activity, $\tilde{u}$, which on average varies by at most ~20% between cruises. Below the thermocline, there is a substantial decrease in $\tilde{u}$ compared to that within the thermocline. The concomitant decrease in ϵ is consistent with our assumed scaling with the velocity scale $\tilde{u}$. To investigate the scaling further, ideally we need observations of well-defined SVS activity that cover a greater variation in $\tilde{u}$, and enough observations to allow a more local (in space and time) examination of the connection between $\tilde{u}$ and ϵ.

Provided the shear generating the turbulence is resolved, our results point to a way to parameterize the unresolved turbulence based on (1), (2), the assumption that $u_t \sim 0.1\tilde{u}$ and the $f(Ri)$ implied by Figure 6. We present observational evidence from a natural environment that the scaling for the vertical length scale ℓ_v varies as (2), at least for sufficiently large N^2 (Figure 5) and that the function $f(Ri)$ has a rather muted variation for small *Ri* (Figure 6). The range of N and *Ri* for which (2) is valid needs to be explored in different flow regimes, but our data suggest that even with $Ri = 0.05$, (2) is valid for sufficiently large N (Figure 5), i.e., the stratification is still important at large shear.

Kunze et al. [1990] derive a form of (1) based on physical principles, in part based on *linear* stability theory. To what extent (5) holds at finite amplitude has not been thoroughly tested. Based on our 2 m averaged data, we find that their vertical length scale, Δz (the thickness of a layer over which $Ri < Ri_{cr}$), is a function of N (Figure 7), but that ℓ_v is probably a more appropriate vertical scale. In addition, the implied variation with Richardson number $f_k(Ri)$, given by (6), increases too rapidly for small *Ri*, and drops off too rapidly for large *Ri* (Figure 6). We also find that by ignoring variations with respect to N, we can fit KPP reasonably well for small *Ri* but not for larger *Ri*. This latter discrepancy is potentially important. We find samples with $Ri > 0.25$ contribute significantly (30%) to the overall mean of κ_v and therefore cannot be ignored. How much this fraction is a consequence of our vertical resolution (2 m) is unclear but we note a possible change in regime for $Ri > 0.25$. With some observational evidence, *Baumert and Peters* [2004] propose four regimes: growing, stationary, decaying, and collapsing turbulence depending on $Ri < 1/4$, $Ri = 1/4$, $1/4 < Ri < 1/2$, and $1/2 < Ri$, respectively. They suggest the radiation of gravity waves needs to be taken into account as an important sink of energy for $Ri \gtrsim 0.25$.

The rich detail of the data set presented here will be useful in guiding future Large Eddy Simulation or Direct Numerical Simulation experimentation to elucidate the controls on the level and scaling of the turbulence. Of particular interest is the relationship between the exterior (SVS) velocity and length scales $\tilde{u}$ and L_S (the vertical scale of the SVSs) and the turbulence scales u_t and ℓ_v. We also need to determine the limits of applicability of the scaling of the average (time or ensemble mean) ϵ and κ_v suggested by the data. Numerical experimentation is challenging, however, because of the large range of length scales involved, from several degrees of latitude down to the turbulent eddies. Formulating a parameterization scheme suitable for conventional ocean or climate models that do not resolve the SVS activity requires the additional knowledge of how $\tilde{u}$ and L_S are related to the larger scale flow and density fields that are resolved in such models.

Lastly, in terms of the dynamics of the equatorial ocean, we note our measurements are confined to the western equatorial Pacific. There is no reason, at the moment, to exclude, or even doubt, the presence of SVSs in the eastern equatorial Pacific. *Peters et al*. [1991] give an example of a "shear wave" inducing turbulence, and similar structures have been seen in high-frequency ADCP measurements in the region (unpublished data). Given the complexity of the flow in the eastern tropical Pacific with a shallower thermocline, faster EUC, and the presence of tropical instability waves, the relative importance of SVS-induced mixing

requires further study. We note, however, that a relatively modest increase in the diffusivity, to account for SVS-induced mixing, produces a considerably larger change in the total vertical diffusivity through feedbacks in the stratification and resolved velocity shear [*Sasaki et al*., 2013].

Appendix A: A Comment on the Estimate of the Mean of a Lognormal Distribution With Noise

If ϵ is lognormally distributed and $y=\ln\epsilon$, then the expected value of ϵ is

$$E(\epsilon)=\exp(\bar{y}+0.5\sigma_y^2) \tag{A1}$$

where $\bar{y}$ and σ_y are the mean and standard deviation of y, respectively. Following the suggestion of D. R. Cox (discussed in *Land* [1972]) we take the 95% confidence limits on $E(\epsilon)$ as

$$[E(\epsilon)\exp(-1.96\gamma), E(\epsilon)\exp(1.96\gamma] \tag{A2}$$

where

$$\gamma=\left[\sigma_y^2/n+\sigma_y^4/2(n+1)\right]^{1/2}$$

and n is the number of samples.

The probability density function of $\log_{10}\epsilon$ for samples with $0.2<Ri<0.3$ (for all N^2) is shown in Figure A1. The estimate (A1) gives $E(\epsilon)=0.89\times10^{-8}$ W kg^{-1} ($\bar{y}=-20.4$ and $\sigma_y^2=3.7$) compared to the arithmetic mean $\bar{\epsilon}=1.01\times10^{-8}$ W kg^{-1}. The p.d.f. of ϵ, however, is noticeably affected by noise centered around $\epsilon=3\times10^{-10}$ W kg^{-1}. The presence of noise will affect the estimate (A1) more than the arithmetic mean and will have

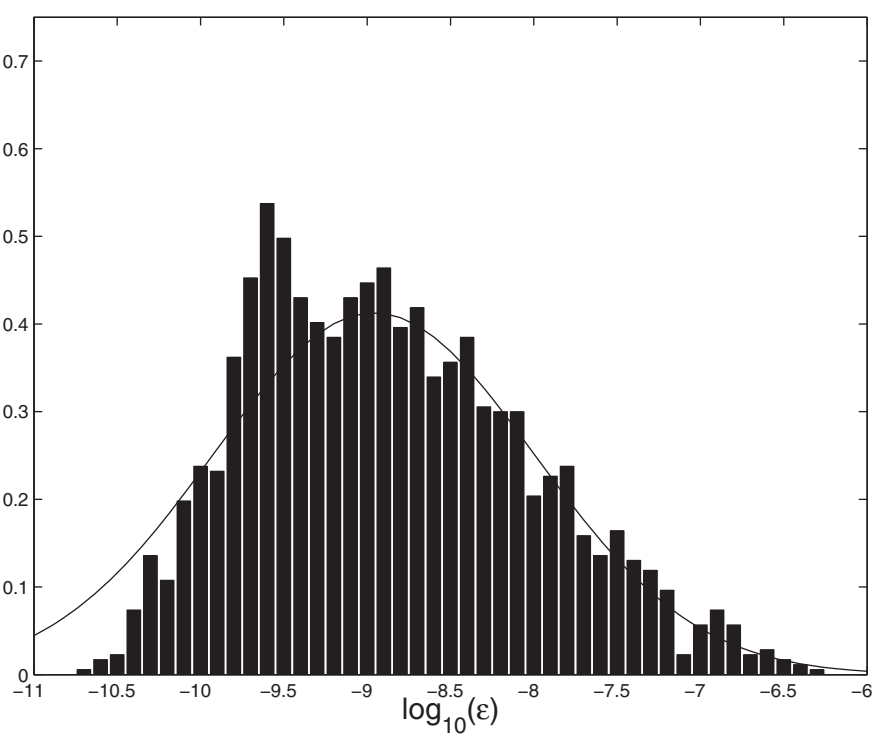

Figure A1. Probability density function of $\log_{10}\epsilon$ for samples with Richardson number, *Ri*, between 0.2 and 0.3. Black curve: one-sided Gaussian fit (see text).

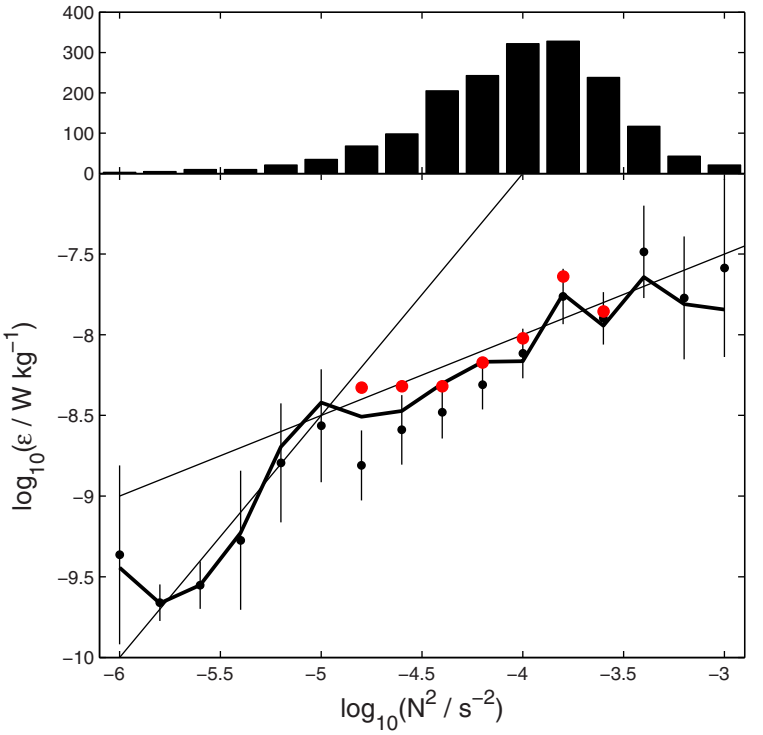

Figure A2. (bottom) Turbulent kinetic energy dissipation rate, ϵ, plotted against $\log_{10} N^2$ for Richardson number, *Ri*, between 0.2 and 0.3. Data taken between the mixed layer and 250 m depth. Black line: arithmetic mean. Black circles with bar: mean assuming data are distributed lognormally with 95% confidence limits. Red circles: mean by fitting a lognormal distribution (see Appendix A). Thin black lines show ϵ varying as N^3 and N. (top) Number of samples in each $\log_{10} N^2$ bin.

implications on the estimates of both $\bar{y}$ and σ_y, producing an overestimate and underestimate, respectively. The thin line in Figure A1 is a Gaussian distribution assuming $\bar{y}=-20.6$ (equivalent to $\epsilon=1.1\times10^{-9}$ W kg^{-1}), obtained by a one-sided least squares fit for $y \geq \bar{y}$, and $\sigma_y^2=5.09$, the latter calculated again from values of $y \geq \bar{y}$. With these values, $E(\epsilon)=1.30\times10^{-8}$ W kg^{-1}, indicating the presence of noise produces an underestimate of the mean ϵ, in this case, of around 70%. This underestimate of the mean is also found when we consider model distributions with noise (not shown).

The estimate $E(\epsilon)$ and confidence limits from (A1) and (A2) are shown in Figure A2 for samples in individual N^2 bins and a fixed value of *Ri*, together with the arithmetic mean from Figure 5. For all but two of the points (at $\log_{10} N^2 = -4.8$ and -4.4), the arithmetic mean falls within the confidence limits of $E(\epsilon)$. There is a suggestion, however, that the slope between $\log_{10} N^2 = -4.8$ and -4.0 is somewhat steeper than the arithmetic mean with $\epsilon \propto N^{1.5}$. From the above, we expect the presence of noise to produce an underestimate in $E(\epsilon)$ as the mean of the distribution approaches the noise level. Indeed, a one-sided Gaussian fit (red dots in Figure A2) gives somewhat elevated values for the mean ϵ compared with $E(\epsilon)$ for smaller N^2. The average width of the confidence interval for the one-sided Gaussian fit is 0.5 which is approximately 30% larger than that for *E*.

Producing a one-sided Gaussian fit to individual $\log_{10} N^2$ bins as used in Figure 5 becomes more difficult as the number of samples decreases (Figure A2, top) and $\bar{y}$ approaches the noise level. In Figure 5, we have plotted those values for which the fit works reasonably well, although we acknowledge that it is unclear how well our assumption that the data are lognormally distributed applies for the smaller values of N^2. The one-sided fit, again, shows $\epsilon \propto N$ for $N^2 > 10^{-5}$, similar to the arithmetic mean, but with an amplitude which is approximately 25% larger for the range of *Ri* considered in Figure 6.

The estimate $E(\epsilon)$ shows a falloff for $N^2 < 10^{-5}$ s^{-2}, similar to the arithmetic mean, although how much the slope is an artifact of averaging values close to the noise level is unclear.

Acknowledgments

This work was supported by the U.S. National Science Foundation under grant OCE1029722, the Japan Agency for Marine-Earth Science and Technology, and the Ministry of Oceans and Fisheries of Korea through the project Ocean Climate Change: Analyses, Projections, and Adaptation. J.H.L. was supported by the National Science Foundation of Korea grant (NRF-2009-C1AAA001–0093065). The R/V Mirai cruises were conducted under the Tropical Ocean Climate Study project of JAMSTEC. We are particularly thankful to the Captains of the R/V Mirai (Akamine and Ishioka) and R/V Kilo Moana (Drewry), their respective crews and marine technical support teams Marine Works Japan Co., Ltd. and Global Ocean Development Inc. (Mirai) and UH OTG (Kilo Moana) for their expertise and enthusiastic help in collecting the data. The data used in this paper are available via Kelvin Richards (rkelvin@hawaii.edu). We thank Bill Symth and an anonymous reviewer for comments that substantially improved the presentation of our results.

References

Bartello, P., and S. M. Tobias (2013), Sensitivity of stratified turbulence to the buoyancy Reynolds number, *J. Fluid Mech.*, *725*, 1–22.

Baumert, H., and H. Peters (2004), Turbulence closure, steady state, and collapse of waves, *J. Phys. Oceanogr.*, *34*, 505–512.

Brethouwer, G., P. Billant, E. Lindborg, and J.-M. Chomaz (2007), Scaling analysis and simulation of strongly stratified turbulent flows, *J. Fluid Mech.*, *585*, 343–368.

Fischer, J., and M. Visbeck (1993), Deep velocity profiling with self-contained ADCPs, *J. Atmos. Oceanic Technol.*, *10*, 764–773.

Godeferd, F. S., and C. Staquet (2003), Statistical modelling and direct numerical simulations of decaying stably stratified turbulence. Part 2. Large-scale and small-scale anisotropy, *J. Fluid Mech.*, *486*, 115–159.

Koop, C. G., and F. K. Browand (1979), Instability and turbulence in a stratified fluid with shear, *J. Fluid Mech.*, *93*, 135–159.

Kunze, E., A. J. Williams III, and M. G. Briscoe (1990), Observations of shear and vertical stability from a neutrally buoyant float, *J. Geophys. Res.*, *95*(C10), 18,127–18,142.

Land, C. E. (1972), An evaluation of approximate confidence interval estimation methods for lognormal means, *Technometrics*, *14*, 145–158.

Large, W. G., J. C. McWilliams, and S. C. Doney (1994), Oceanic vertical mixing: A review and model with a nonlocal boundary layer parameterisation, *Rev. Geophys.*, *32*, 363–403.

Lee, C., K. I. Chang, J. H. Lee, and K. J. Richards (2014), Vertical mixing due to double diffusion in the tropical Western Pacific, *Geophys. Res. Lett.*, *41*, 7964–7970, doi:10.1002/2014GL061698.

McDougall, T. J., and B. R. Ruddick (1992), The use of ocean microstructure to quantify both turbulent mixing and salt-fingering, *Deep Sea Res., Part A*, *39*, 1931–1952.

Moum, J. N., et al. (1989), Mixing in the equatorial surface layer and thermocline, *J. Geophys. Res.*, *94*, 2005–2021.

Oakey, N. S. (1982), Determination of the rate of dissipation of turbulent energy from simultaneous temperature and velocity shear microstructure measurements, *J. Phys. Oceanogr.*, *12*, 256–271.

Osborn, T. R. (1982), Estimates of the local rate of vertical diffusion from dissipation measurements, *J. Phys. Oceanogr.*, *10*, 83–89.

Peltier, W. R., and C. P. Caulfield (2003), Mixing efficiency in stratified shear flows, *Annu. Rev. Fluid Mech.*, *35*, 135–167.

Peters, H., M. C. Gregg, and J. M. Toole (1988), On the parameterisation of equatorial turbulence, *J. Geophys. Res.*, *93*, 1199–1218.

Peters, H., M. C. Gregg, and T. B. Sanford (1991), Equatorial and off-equatorial fine-scale and large-scale shear variability at 140°W, *J. Geophys. Res.*, *96*(C9), 16,913–16,928.

Peters, H., M. C. Gregg, and T. B. Sanford (1995), On the parameterisation of equatorial turbulence: Effect of fine-scale variations below the range of the diurnal cycle, *J. Geophys. Res.*, *100*(C9), 18,333–18,348.

Polzin, K. (1996), Statistics of the Richardson number: Mixing models and finestructure, *J. Phys. Oceanogr.*, *26*, 1409–1425.

Polzin, K., E. Kunze, J. Hummon, and E. Firing (2002), The finescale response of lowered ADCP velocity profiles, *J. Atmos. Oceanic Technol.*, *19*, 205–224.

Richards, K. J., and N. R. Edwards (2003), Lateral mixing in the equatorial Pacific: The importance of inertial instability, *Geophys. Res. Lett.*, *30*(17), 1888, doi:10.1029/2003GL017768.

Richards, K. J., Y. Kashino, A. Natarov, and E. Firing (2012), Mixing in the western equatorial Pacific and its modulation by ENSO, *Geophys. Res. Lett.*, *39*, L02604, doi:10.1029/2011GL050439.

Rohr, J., E. Itsweire, K. Helland, and C. Van Atta (1988), Growth and decay of turbulence in a stably stratified shear flow, *J. Fluid Mech.*, *195*, 77–111.

Sasaki, W., K. J. Richards, and J.-J. Luo (2013), Impact of vertical mixing induced by small vertical scale structures above and within the equatorial thermocline on the tropical Pacific in a CGCM, *Clim. Dyn.*, *41*(2), 443–453, doi:10.1007/s00382-012-1593-8.

Shay, T. J., and M. C. Gregg (1986), Convectively driven turbulent mixing in the upper ocean, *J. Phys. Oceanogr.*, *16*(11), 1777–1798.

Smyth, W. D., and J. N. Moum (2000), Length scales of turbulence in stably stratified mixing layers, *Phys. Fluids*, *12*(6), 1327–1342.

Smyth, W. D., and J. N. Moum (2013), Marginal instability and deep cycle turbulence in the eastern marginal instability and deep cycle turbulence in the equatorial Pacific Ocean, *Geophys. Res. Lett.*, *40*, 6181–6185, doi:10.1002/2013GL058403.

Smyth, W. D., J. N. Moum, and D. R. Caldwell (2001), The efficiency of mixing in turbulent patches: Inferences from direct simulations and microstructure observations, *J. Phys. Oceanogr.*, *31*, 1969–1992.

Smyth, W. D., J. D. Nash, and J. N. Moum (2005), Differential diffusion in breaking Kelvin–Helmholtz billows, *J. Phys. Oceanogr.*, *35*, 1004–1022.

Taylor, G. I. (1935), Statistical theory of turbulence: Parts I–II, *Proc. R. Soc. London, Ser. A*, *151*, 421–464.

Waite, M. L., and P. Bartello (2004), Stratified turbulence dominated by vortical motions, *J. Fluid Mech.*, *517*, 281–308.

Wesson, J. C., and M. C. Gregg (1994), Mixing at Camarinal Sill in the Strait of Gibraltar, *J. Geophys. Res.*, *99*(C5), 9847–9878.

Whalen, C. B., L. D. Talley, and J. A. MacKinnon (2012), Spatial and temporal variability of global ocean mixing inferred from Argo profiles, *Geophys. Res. Lett.*, *39*, L18612, doi:10.1029/2012GL053196.

Zaron, E. D., and J. N. Moum (2009), A new look at Richardson number mixing schemes for equatorial ocean modeling, *J. Phys. Oceanogr.*, *39*, 2652–2664.